
This is an electronic reprint of the original article.
This reprint may differ from the original in pagination and typographic detail.

Ullah, Rizwan; Akmal, Jan Sher; Laakso, Sampsa; Niemi, Esko

Anisotropy of additively manufactured 18Ni-300 maraging steel: Threads and surface characteristics

DOI:

[10.1016/j.procir.2020.04.059](https://doi.org/10.1016/j.procir.2020.04.059)

Published: 22/09/2020

Document Version

Publisher's PDF, also known as Version of record

Please cite the original version:

Ullah, R., Akmal, J. S., Laakso, S., & Niemi, E. (2020). *Anisotropy of additively manufactured 18Ni-300 maraging steel: Threads and surface characteristics*. 68-78. Paper presented at CIRP Conference on Manufacturing Systems, Chicago, United States. <https://doi.org/10.1016/j.procir.2020.04.059>

This material is protected by copyright and other intellectual property rights, and duplication or sale of all or part of any of the repository collections is not permitted, except that material may be duplicated by you for your research use or educational purposes in electronic or print form. You must obtain permission for any other use. Electronic or print copies may not be offered, whether for sale or otherwise to anyone who is not an authorised user.

53rd CIRP Conference on Manufacturing Systems

Anisotropy of additively manufactured 18Ni-300 maraging steel: Threads and surface characteristics

Rizwan Ullah^{a*}, Jan Sher Akmal^a, Sampsa Laakso^a, Esko Niemi^a

^a*Department of Mechanical Engineering, Aalto University, Espoo, Finland*

* Corresponding author. Tel.: +358-40-3558445; Email address: Rizwan.ullah@aalto.fi

Abstract

The purpose was to evaluate part properties of additively manufactured 18Ni-300 maraging steel in a unified set-up when the printing orientation and the heat treatment were independently changed. Though the hardness, shrinkage, and drilling thrust force showed isotropic behavior to a certain extent, anisotropy was observed in the flatness, surface roughness, dross, and thread profiles. Solution treatment increases the surface roughness and reduces the flatness, surface hardness, drilling thrust force, and thread quality to some extent. Aging treatment significantly increases the surface hardness and yet still allows good-quality threads to be cut. The study aids designers in establishing and corroborating design for additive manufacturing.

© 2020 The Authors. Published by Elsevier B.V.

This is an open access article under the CC BY-NC-ND license (<http://creativecommons.org/licenses/by-nc-nd/4.0/>)
Peer-review under responsibility of the scientific committee of the 53rd CIRP Conference on Manufacturing Systems

Keywords: 3D printing; Direct metal laser Sintering (DMLS); internal threads; printing inclination; heat treatment; anisotropy

1. Introduction

Additive manufacturing (AM) can produce complex features with intricate details. AM products are used as functional parts in almost all high-tech industries, including the aerospace, automotive, tooling, and medical industries [1–3]. In the AM process, material is typically joined layer by layer to make parts from three-dimensional (3D) model data as opposed to subtractive and formative manufacturing methodologies [4].

Manufacturing defects in the form of pores [5], dross [6], warpage [7], high surface roughness, and anisotropy in mechanical properties pose some challenges at the user end. Volume shrinkage occurs during laser densification in metal powder bed fusion (m-PBF) process [8,9] and can affect as-built (AB) part dimensional stability. Subtractive manufacturing techniques are thus essential for achieving engineering tolerances for critical components. Efforts are being made to combine additive and subtractive manufacturing in one place so as to obtain finished mechanical parts with the highest accuracy [10–12].

Maraging steel exhibits high strength and wear resistance properties which make it suitable for many applications in the aircraft and tooling industries. Additively manufactured maraging steel and its machining are being vastly researched at the moment [13–16] owing to its high strength, derived from martensite, and toughness, derived from the aging process. AM technologies allow the production of metallic parts, in particular 18Ni-300 maraging steel using the powder bed fusion (PBF) process, in which thermal energy is used to selectively melt the metallic powder particles for fusion.

Optimization of the most crucial PBF process parameters; laser power, scanning speed, energy density, layer thickness, laser spot diameter, and melt pool overlap, can significantly improve dimensional stability and influence mechanical properties, as indicated by previous studies [17–19]. OEM optimizes these printing parameters in PBF machines to ensure repeatability. EOS GmbH has commercialized standard parameters that are optimized for cost, build time,

or performance in terms of better surface characteristics and uniform material properties. The aforementioned PBF process parameter sets are characterized with these standard commercial parameter names.

Additively manufactured maraging steel shows higher tensile and yield strength properties in the horizontal direction compared to the vertical direction, implying anisotropy [20]. The effect of the build direction on its material properties is a crucial phenomenon in the PBF process because of the layerwise effect. For instance, the surface roughness measured in the vertical build direction is greater compared with the horizontal build direction [16].

For maraging steel, the solution treatment process can reduce the anisotropic effect inherited from the PBF process [21]. The aging process, on the other hand, can significantly enhance the mechanical properties (strength and hardness) of AB maraging steel. Typically, AB maraging steel is solution-treated (ST) before aging is performed, which in turn imparts high strength properties. In the aging process, maraging steel is held below the austenitization temperature (~ 560 °C), typically for six hours, which promotes hindering of precipitation and imparts high strength properties [22] as a result of the intermetallic precipitates. Direct aging can also be performed on AB maraging steel components and has been reported to lead to strength properties comparable with those of ST-aged parts [23]. Horizontally built components have shown a higher yield and ultimate strength compared to vertically built components, indicating anisotropy [23].

To minimize the manufacturing defects that characterize the PBF process, subtractive manufacturing techniques are adopted. The machining characteristics of additively manufactured maraging steel showed tensile residual stresses near the machined surface built up during the PBF process which were not present in wrought components [15]. Tool wear has been observed to be lower for ST samples compared to AB and aged additively manufactured maraging steel [16]. The machining of high-strength maraging steel can sometimes produce burrs attached to the surface that can affect the surface quality [24].

PBF process capabilities are often expressed in terms of material properties along horizontal and vertical orientations to highlight the anisotropy induced by the build direction. There are only a few studies that explore the effect of various printing inclinations on part accuracy in terms of surface properties (flatness, surface roughness) and dimensional accuracy affected by dross and shrinkage for additively manufactured maraging steel. Internal thread manufacturing, flatness error in as-built plates, shrinkages, and the effect of pre-holes on thread quality have scarcely been investigated for additively manufactured maraging steel. In this research, these gaps are filled by examining the quality of threads along various printing inclinations. The machining allowances required for internal threads are also discussed. This experimental study explores the dependence of surface roughness, flatness, hardness, shrinkages, and

drilling thrust forces and thread quality as a function of the printing inclination.

The aim of this study is to evaluate part properties, i.e., flatness, surface roughness, surface hardness, pre-hole shrinkage, drilling thrust force, and thread profiles in a unified setup when the printing orientation and the heat treatment were independently changed.

2. Experimental methods

This study investigated the anisotropy in additively manufactured maraging steel (18% Ni Maraging 300/ European 1.2709/German X3NiCoMoTi [21]) using the unified method of evaluating part properties [25].

2.1 Test plate design for additive manufacturing

Figure 1 shows the geometry of the additively manufactured test plate containing pre-holes. The rectangular flat plates (8-mm thick) were designed using the Creo Parametric (4.0, PTC, Needham, MA, USA) software. The plates contained pre-holes that deviated from the nominal diameter of 4.2 mm and 6.8 mm, which are recommended for tapping M5 and M8 threads, respectively.

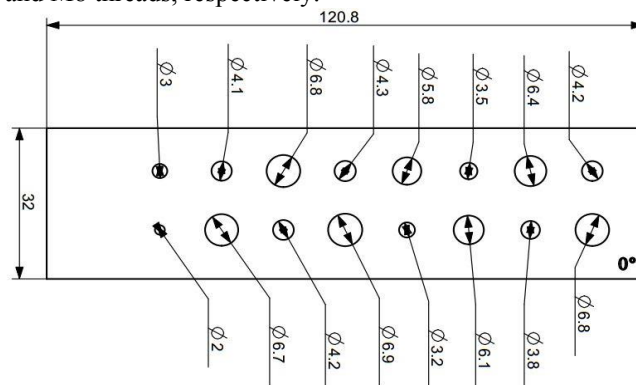


Figure 1: The schematic of the test plate in millimeters [25]

The pre-hole increment is determined on the basis of the minimum feature size in the XY-plane of the AM machine. The left-hand region of the plate is intended for direct drilling into the solid material. The thickness of all the plates was 8 mm.

The machining allowances determined by the pre-hole increments are listed in Table 1 for the two pre-hole diameters, i.e., 4.2 mm and 6.8 mm.

Table 1: Machining allowances of the 4.2-mm and 6.8-mm pre-hole diameters [25]

Pre-hole diameter (mm)	Machining allowance for 4.2-mm drill	Pre-hole diameter (mm)	Machining allowance for 6.8-mm drill
4.3	+0.1	6.9	+0.1
4.2	0.0	6.8	0.0
4.1	-0.1	6.7	-0.1
3.8	-0.4	6.4	-0.4
3.5	-0.7	6.1	-0.7
3.2	-1.0	5.8	-1.0
2.0	-2.2	3.0	-3.8
Direct drilling	-4.2 mm	Direct drilling	-6.8 mm

The test plates were additively manufactured at five printing inclinations (0° , 30° , 45° , 60° , & 90°), as shown in Figure 2. No primary heat treatment was employed for the set of as-built (AB) plates shown in Figure 4, while for the other set, the plates were solution-treated (ST) for two hours at 940°C followed by rapid air-cooling to a temperature below 32°C with a cooling rate of $20\text{--}60^\circ\text{C}/\text{min}$.

Two plates were manufactured at a 90° orientation, which were aged (for a holding time of six hours at 490°C , followed by air cooling) from the AB and ST state, in order also to evaluate the effect of the secondary heat treatment process on the hardness and thread profile. Subsequently, the two additional plates printed at a 90° orientation, one per print job (AB and ST), underwent aging as the secondary heat treatment process. The AB plate was directly aged (AB-aged), and the ST plate was aged (ST-aged) after solution treatment.

The global AM parameters are presented in Table 2, and the printing parameters are presented in Table 3.

The printing parameters, i.e., laser power, scanning speed, hatch distance, and scanning strategy, are defined by the Performance 2.0 parameter set [26], which was uniform for both sets. The printing strategy included outer contours and a rotation of the laser scanning path through 67° for successive layers. The stripes were exposed against the flow of nitrogen gas. The manufacturing repeatability is ensured by the MS1 performance 2.0 parameter set. The X- and Y-spacing between consecutive supports was 0.6 mm , and the rotation angle was 45° . The exposure parameters for the supports are different from the bulk manufacturing because the supports are typically exposed in single lines and are optimized for single walls.

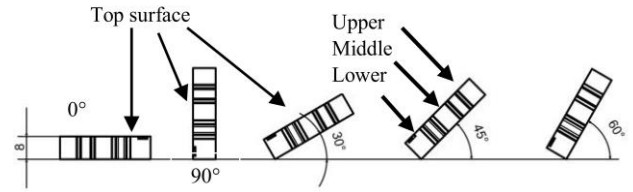


Figure 2: The printing inclinations [25]

2.2 Flatness error

The flatness error was measured on the top surface of the plates using the Ruby CMM model 444 (CE Johansson AB, Eskilstuna, Sweden), which had an accuracy of $20\ \mu\text{m}$. The flatness measurement consisted of 60 data points that were randomly selected on the top surface of the plate. Three measurements were recorded for each plate.

The test plates were removed from the substrate using a bandsaw. The supports were removed by milling. The design intent ensured that the pre-holes were not supported with any support structures.

2.3 Surface roughness

The Form Talysurf i120 (Taylor Hobson, Leicester, United Kingdom) was used to measure the surface roughness of the top surface (R_a value) of the plates using a stylus-type measuring tool. The measurements followed the EN ISO 4288 standard, and a cut-off length of 2.5 mm was selected.

2.4 Hardness

The hardness was measured on the top surface of the plates with the Rockwell hardness (HRC) scale using the SwissMax 300 (Gnehm, Thalwil, Switzerland) equipment.

Table 2: EOS global parameters used in this study

ISO/ASTM AM method	Machine	Software	Global additive manufacturing parameters					Support structure parameters	Post-processing
			Material	Particle size	Chamber atmosphere	Plate layer thickness			
Powder bed fusion	EOS M290	EOSPRINT	Maraging steel MSI	$15\text{--}63\ \mu\text{m}$	Nitrogen	$40\ \mu\text{m}$	Type: Block supports Software: EOSPRINT-1.7 EOS Standard parameter Performance 2.0	Machining for support removal	

Table 3: Additive manufacturing printing parameters

Additive manufacturing parameters						
Original EOS Parameter Set	Energy input	Substrate Temperature	Recoater angle	Plate orientation angle	Post processing: Heat treatment	
					Primary	Secondary (90° orientation)
Performance 2.0	$67.5\ \text{J}/\text{mm}^3$	40°C	5°	$0^\circ, 30^\circ, 45^\circ, 60^\circ, \& 90^\circ$	As-built (AB)	Aged
Performance 2.0	$67.5\ \text{J}/\text{mm}^3$	40°C	5°		Solution treated (ST)	Aged

2.5 Hole diameter

The additively manufactured pre-hole diameter was measured for each pre-hole using a hole gauge set and a digital micrometer.

2.6 Thrust force measurement

The plates were drilled and subsequently tapped using an MX-520 vertical machining center (Matsuura, Fukui-city, Japan). The axial drilling thrust force was measured using a Kistler 9271 piezoelectric sensor. The experiments were conducted at room temperature. The coordinates of the printed pre-holes were determined manually using a centering microscope. The cutting parameters were selected in accordance with the recommendations of the tool manufacturer (Table 4), particularly, the Walter Titex [27] tools and machining parameters, for the AB and ST plates.

Table 4: OEM recommended tools

	Product Name	f^*	v_c^{**}	Point angle	No. of Flutes
Drills	A3293TTP-4.2	0.078	200	140°	2
	A3293TTP-6.8	0.11	150	140°	2
	Product Name	Tapp material	V_c	Tapp coating	Pitch (mm)
Taps	S2021305-M5	HSS	0.063	TiN	0.8
	S2021305-M8	HSS	0.01	TiN	1.25

*Feed=f (mm/rev)

**Cutting speed = v_c (mm/min)

2.6.1 Tools for aged maraging steel

To compensate for the underlying microstructural morphology and the subsequent mechanical properties of the aging process, compatible tools were used for drilling and tapping, as listed in Table 5.

Table 5: Drilling and Tapping tools used for aged maraging steel

Operation	Cutting tool (Product name)	Cutting speed (m/min)	Feed (mm/rev)
M5	Direct Drilling Dijet 4.2-mm drill DZ-DHS0420	60	0.08
	Tapping 8031106-M5 Tap	5.3	0.8
M8	Direct Drilling Dijet 4.2-mm drill DZ-DHS0420	60	0.08
	Tapping 8031106-M8 Tap	8.5	1.25

All the M5 pre-holes were cut using a 2-mm milling tool [YONNEX Y545] to obtain a nominal diameter of 4.2 mm. In the case of direct drilling of solid material (no pre-hole) to obtain the 4.2-mm diameter, a Dijet 4.2-mm drill was used.

In the case of directly cutting a 6.8-mm hole in aged maraging steel, a Dijet 4.2-mm drill was used. Then it was milled with a 4-mm milling tool [YONNEX Y545] to obtain a diameter of 6.8 mm.

Finally, the nominal holes, i.e., 4.2 and 6.8 mm, whether directly drilled or milled, were tapped using the Walter Titex tools to obtain M5 and M8 respectively.

2.7 Thread-stripping force

ISO standard 899-2 standard guidelines were followed to design a custom-made thread-stripping setup [25] for the stripping of internal threads in maraging steel plates. An axial tensile force was applied to nut threads made in a horizontal plate, using a 12.9 bolt. The additively manufactured plate was clamped to the flat stationary bed with another rectangular plate using four bolts. The tensile machine had a capacity to apply a force of 50 kN. The thickness of the plates was reduced to 5 mm for the thread stripping to reduce the thread engagement length and hence requiring less stripping force compared to 8 mm thickness. This would allow more tensile force available for stripping of threads made in maraging steel.

2.8 Thread profiles

Following the tapping of the M5 and M8 internal threads in the maraging steel, a cross-section of the threads was cut as shown in Figure 3 using a ROBOFIL 440 (Charmilles, Nürtingen, Germany) EDM wire cut machine. The samples were mechanically prepared by first using SiC grinding paper with a P 2000 FEPA grit size. Then the samples were polished with 1- μ m diamond paste. An etchant with the composition shown in Table 6 was used to reveal the micro-scale details of the surfaces. The samples were etched for two minutes. An objective magnification of 10X was used for observing the thread profiles under an optical microscope. The individual pictures were stitched together to show the continuous threads using the Adobe Photoshop (Adobe Inc., version 21.0.2, San Jose, California, USA) software.



Figure 3: The sectioned internal threads for optical microscopic imaging

Table 6: The composition of the etchant

Material	Amount
Water	50 ml
Ethyl alcohol	50 ml
Methyl alcohol	50 ml
Hydrochloric acid	50 ml
CuCl ₂	1 g
FeCl ₃	2.5 g
HNO ₃	2.5 mL

3. Results and Discussion

Figure 4 shows the additively manufactured maraging steel AB plates at five printing inclinations.

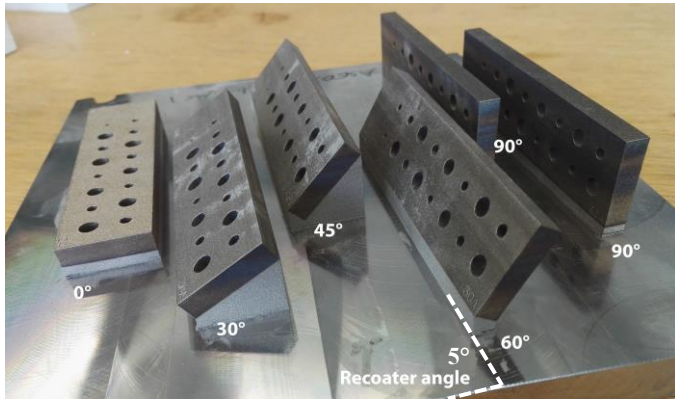


Figure 4: The additively manufactured maraging steel AB plates at five printing inclinations

3.1 Flatness error

Figure 5 shows the flatness error of the AB plates before and after removal from the substrate. This error occurred as a result of the buildup of large thermal gradients during the rapid melting and cooling of the melt pool in the PBF process. The rapid re-solidification induces large residual stresses with the potential of producing warped surfaces (flatness error).

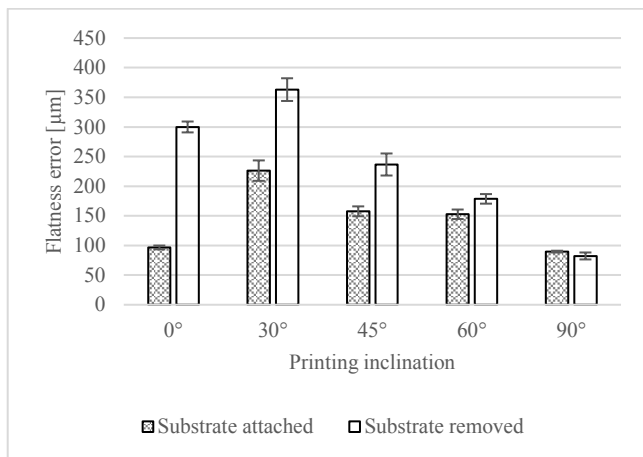


Figure 5: The flatness error of the AB plates

The flatness error was at its minimum at a 90° inclination since a larger portion of the solid plate supported itself and aided efficient heat transfer to the substrate compared with the other printing inclinations. Comparatively, the heat transfer to the substrate at other printing inclinations has a higher dependency on support structures, which have the form of a square grid. Further, the maximum energy input per layer is minimal at a 90° inclination as a result of the smallest cross-sectional area of the melted layer. The second-smallest flatness error was observed at a 0° inclination. This is because of the maximum cross-sectional area of the support structures, which enhances the heat transfer capability and anchoring of the plate to the substrate compared to inclinations of 30° to 60°. The flatness error decreases from 30° to 60° because the cross-sectional area of the supports and maximum energy per layer decrease during this changeover. In this particular case, the reduced cross-sectional area of the supports suggests that the

solid material of the plate has a greater capability of supporting itself and aiding heat sink.

After the removal of the plates from the substrate, the flatness error was intensified with a similar trend. The increase in the amplitude of the flatness error is comparable to the residual stresses. When the substrate was intact, the support structures held the plates to the substrate against the thermal stresses. Their removal from the substrate further intensified the warpage of the top surfaces of the plates.

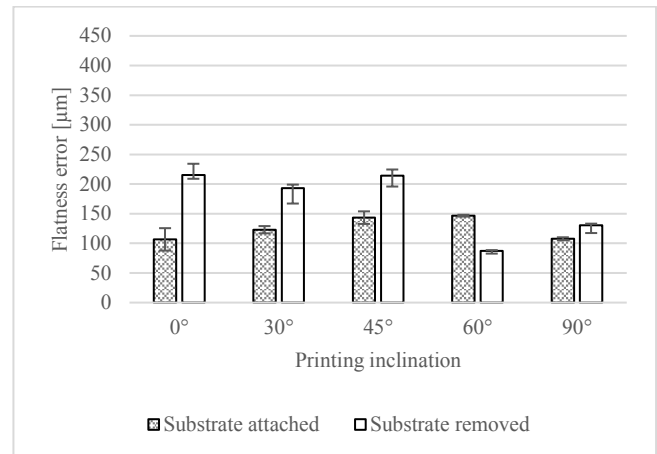


Figure 6: The flatness error of the ST plates

The flatness error reduces significantly for ST plates compared to AB plates, as can be seen from Figure 6. The decrease is caused by the stress relief resulting from the solution treatment process before the plates were removed from the substrate. Evidently, a higher level of flatness error without heat treatment has a greater tendency to decrease with heat treatment than a lower level of flatness error owing to stress relief.

Overall, even though the flatness error at a 90° inclination may be at its minimum, the duration of the print for this individual plate would be the highest compared to the plates printed at other inclinations. The print duration would increase from a 0° to a 60° inclination, which would accumulate additional costs. Thus, trade-offs between the flatness error, duration of the printing, and cost should be considered when selecting the orientation of a part.

3.2 Surface Roughness

The surface roughness of the AB and ST plates is shown in Figure 7. Though identical printing parameters were employed for both the AB and ST plates, the surface roughness of the ST plates was higher as a result of the oxidation effect occurring at elevated temperatures during the solution treatment process.

In the case of the AB plates, the surface roughness decreases from a 30° to a 60° inclination as a result of the staircase effect coupled with powder conglomeration, which is shown in Figure 8. When a printing inclination changes from 30° to 60°, the perpendicular distance from the measurement surface of the plate to the inner corner of the staircase decreases. Further, a substrate temperature of 40 °C can cause conglomeration of

powder particles to the skin of the plate which is in contact with the powder bed during the build cycle. During the transition from a 30° to 60° inclination, the surface area that is perpendicular to the build direction in Figure 8 decreases. A smaller surface area in contact with the powder bed enables a lower surface roughness as a result of a lower intensity of the powder conglomeration. The plate inclined at a 90° inclination has a slightly lower surface roughness because it is not affected by the staircase effect. The plate at a 0° inclination consists of the lowest surface roughness because it is not affected by the stair-case effect and it has the lowest susceptibility to powder conglomeration owing to an up-skin exposure parameter.

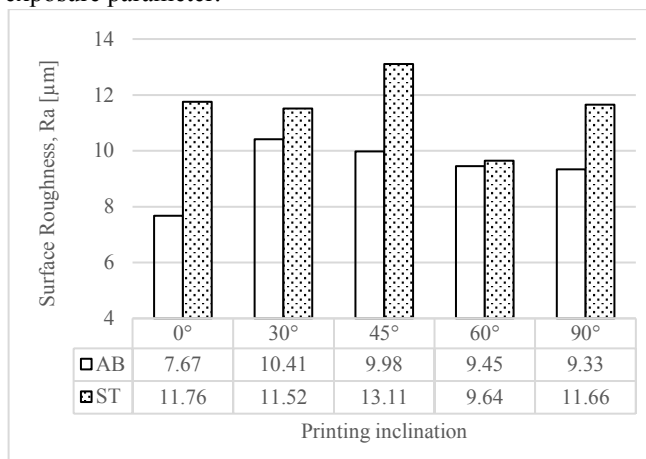


Figure 7: The surface roughness comparison of the AB and ST plates

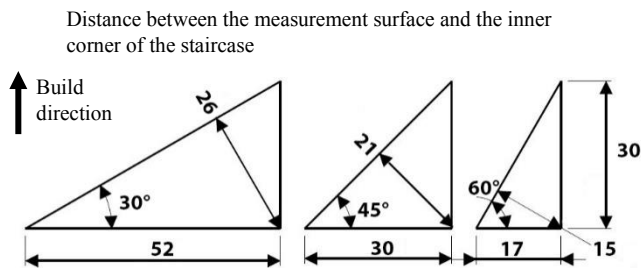


Figure 8: Schematics of the staircase effect at a 30°, 45°, and 60° inclination [25]

3.3 Surface hardness

The AB plates were harder compared to the ST plates owing to the presence of fine grains resulting from the rapid melting and solidification. These results are in line with previous studies. Figures 9 and 10 present the hardness of the AB and ST plates as a function of the printing inclination, measured in three regions of the plate as indicated by Figure 2. The error bars represent the experimental standard deviation. In the case of the AB plates, the surface hardness is quite consistent, which indicates isotropic behavior. The average hardness of all measurement regions as a function of the print inclination is 36.25 HRC \pm 0.44 HRC and contains a range of 1.13 HRC.

Following the solution treatment, the hardness reduces by around 20% owing to the disappearance of fine grain boundaries. The overall results indicate that the hardness is not significantly affected at different heights of the measurement

regions from the substrate and seems to be independent of the print inclination. The average hardness of all measurement regions as a function of the print inclination is 29.00 HRC \pm 0.37 HRC and contains a range of 0.92 HRC.

The average hardness of the AB-aged and ST-aged plates is 53.94 \pm 0.46 HRC and 54.62 \pm 0.34 HRC, respectively, as a result of the formation of intermetallic precipitate [17]. Following the aging process, the hardness of the AB plate increases by approximately 48%. Similarly, after the aging process, the hardness of the ST plate increases by about 86%. Eventually, the hardness of both the AB and ST plates becomes uniform after the aging process.

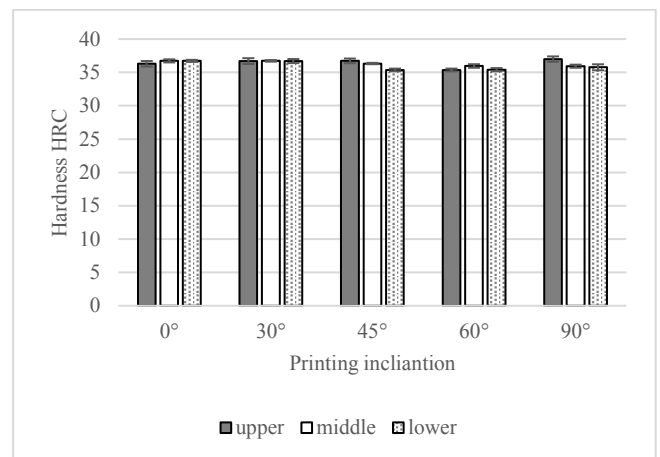


Figure 9: Hardness with regard to printing inclinations at three measurement regions in the AB plates

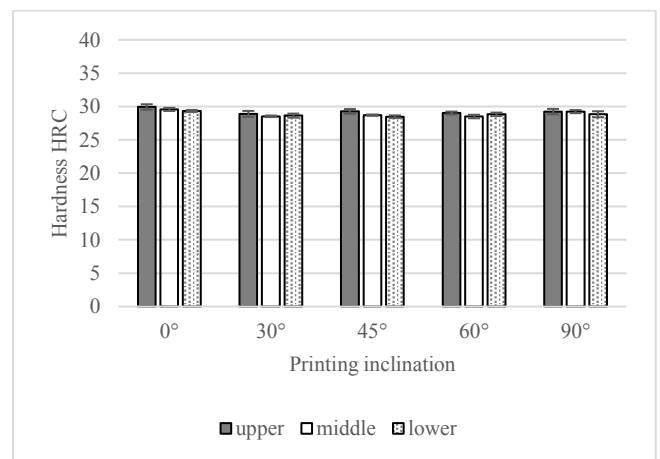


Figure 10: Hardness variation with regard to printing inclinations in three measurement regions of the ST plates

3.4 Pre-hole shrinkage

All the pre-holes had shrunk after the PBF process. Thus, the final diameter was smaller than the nominal diameter prescribed in the CAD model. The shrinkage was caused by the thermal contraction resulting from the large thermal gradients. The shrinkage measurements were affected by the partial melting of powder particles (size: 15-63 μ m) to the down-skin surfaces, resulting in the formation of dross. Figure 11 depicts the measurement method for calculating the dross and shrinkage. Dross is shown by the black region under the

down-skin surface. The difference between the measured diameter (d_1) and nominal diameter represents the shrinkage. The measured diameter d_2 is subtracted from d_1 to calculate the formation of dross.

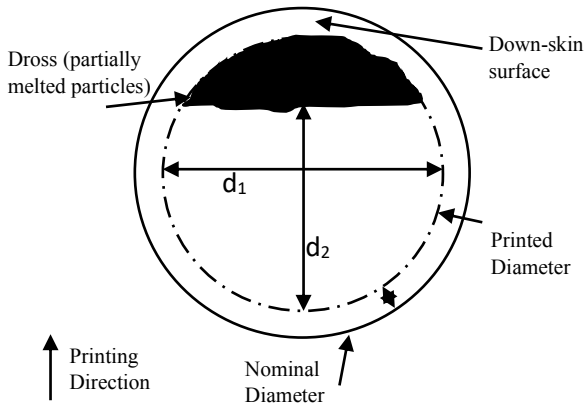


Figure 11: The pre-hole schematic depicting dross and shrinkage [25]

Figures 12 and 13 compare the shrinkage measured in the AB and ST plates for the 4.2- and 6.8-mm pre-holes as a function of the printing inclination.

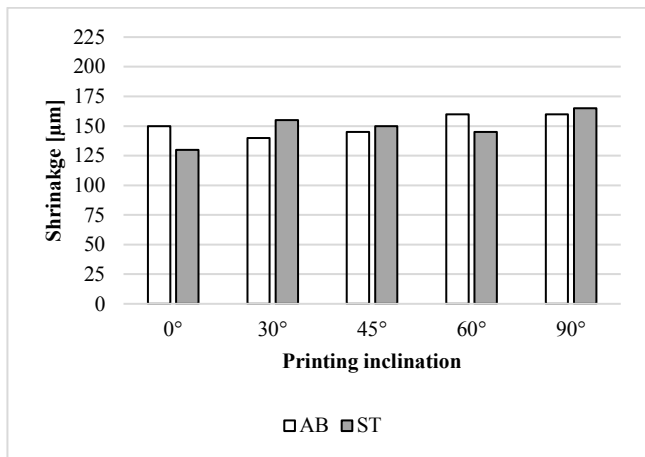


Figure 12: The shrinkage with respect to the printing inclination of the 4.2-mm pre-hole

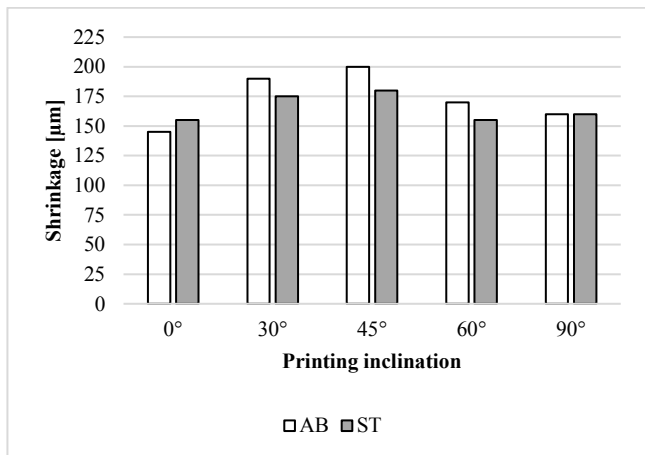


Figure 13: The shrinkage with respect to the printing inclination of the 6.8-mm pre-hole

The shrinkage does not appear to be affected significantly by the solution treatment, and hence, the pre-holes have retained

their diameters. It can be implied that despite the stress-relieving effect caused by the solution treatment, the geometric dimension of the pre-holes remains unaltered, with an average difference of 8% after heat treatment. An average 13% increase in the shrinkage was observed for the 6.8-mm pre-hole compared to the 4.2-mm pre-hole.

On the other hand, the dross increases significantly as the printing inclination angle increases. As the slope of the down-skin surface of the pre-hole increases with an increase in printing inclination, the lack of support structures hinders the heat transfer capability at the down-skin surface. As a result, dross starts to grow at the down-skin surfaces. The ST plates follow a similar trend to that of the AB plates. An identical formation of dross was observed for the 6.8-mm pre-hole.

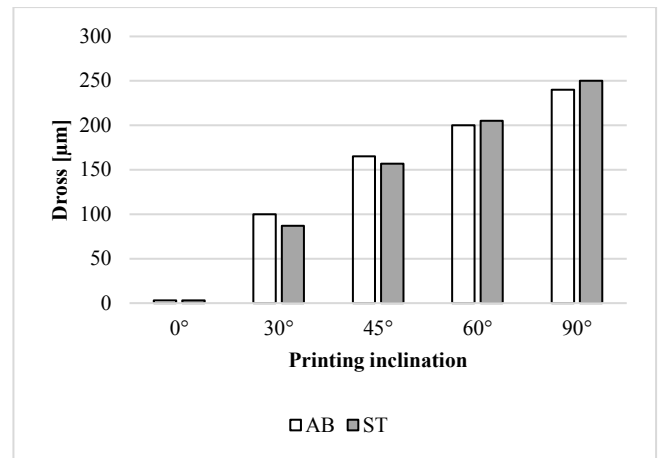


Figure 14: Dross as a function of the printing inclination for the 4.2-mm pre-hole

3.5 Thrust force measurement

Figure 15 and 16 show 3D contour graphs of the axial drilling thrust force of the 4.2-mm and 6.8-mm drills with color codes as a function of the pre-hole sizes and printing inclinations of the AB plates.

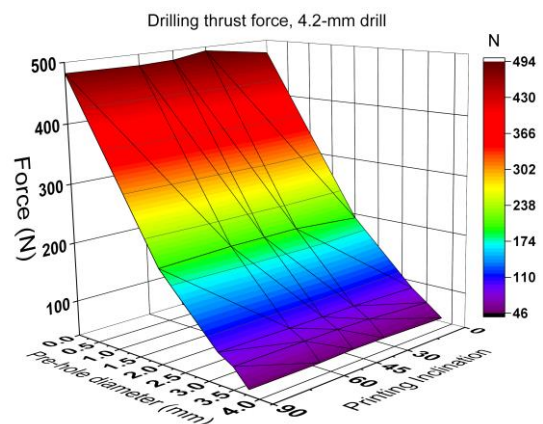


Figure 15: The drilling thrust force of the 4.2-mm drill with respect to the pre-hole diameter and printing inclination of the AB plates

The drilling thrust force does not fluctuate significantly when the printing inclination changes, as shown by the uniform

mesh boundaries. The insignificant variation in the drilling thrust force is most probably due to the alignment error and drill wandering [28]. Further, the thrust force decreases significantly with an increase in the diameter of the pre-hole owing to the lower amount of material removed. Since the drilling parameters (cutting speed, feed) were constant, the drilling thrust force largely depended on the diameter of the pre-hole.

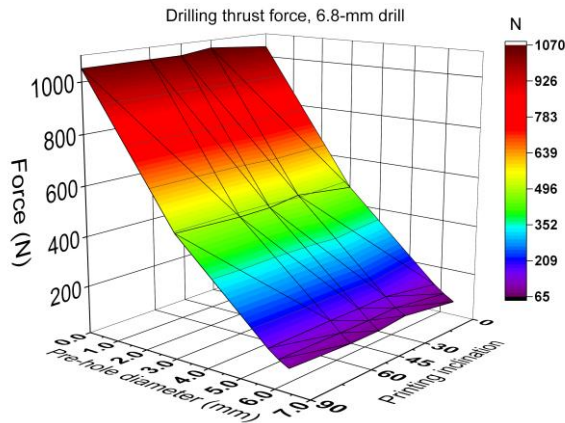


Figure 16: The drilling thrust force of the 6.8-mm drill with respect to the pre-hole diameter and printing inclination of the AB plate

Figure 16 shows that a pre-hole diameter from 3 mm to 6.4 mm (machining allowance of 3.8 mm and 0.4 mm) for a 6.8-mm drill can cut down the drilling thrust force by 54% to 92% compared to direct drilling. Similarly, the drilling force can be reduced by from 59% to 90% with a pre-hole diameter from 2 mm to 3.8 mm (machining allowance of 2.4 mm and 0.4 mm) for the 4.2-mm drill. To this end, introducing pre-holes can significantly reduce the axial drilling thrust force, which otherwise can be critical for the structural integrity of the additively manufactured parts. Particularly, in the case of high-strength maraging steel, the reaction forces are expected to be significantly higher.

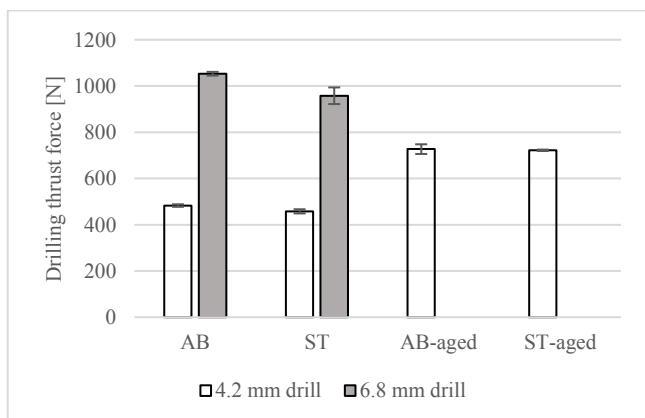


Figure 17: A comparison of the drilling thrust force without pre-holes

Figure 17 presents a comparison of the average axial thrust force for direct drilling in the AB plates, ST plates, AB-aged plate, and ST-aged plate. The drilling thrust force reduces by approximately 5% for the 4.2-mm drill and 8% for the 6.8-mm drill after solution treatment. The decrease in the thrust force

can be associated with the reduced hardness of the ST plates, resulting in lower reaction forces.

The drilling thrust force increases by approximately 51% for the AB-aged plate compared to the AB plates. Similarly, it increases by around 58% for the ST-aged plate compared to the ST plates. Both plates yielded a similar average drilling thrust force after the aging process. This implies that the aging treatment produces identical mechanical properties for the AB-aged and ST-aged plates, which was also indicated by the similar hardness results.

A large drilling force can increase tool wear and defects. To avoid large thrust forces, it is recommended to print a pre-hole and possibly reduce the penetration rate (cutting speed and feed). Additionally, a reduction in the thrust force can ensure that the features, i.e., thin walls with low strength capability remain intact.

3.6 Thread stripping

The attempt to evaluate the thread-stripping force was unsuccessful owing to the high strength of the maraging steel and the fracture of the stripping bolts of class 12.9 defined by the ASTM F568M-07 standard. Figure 18 shows the broken bolts when the internal threads made in the maraging steel were stripped. The bolts broke at a force of 46 kN, indicating high thread strength.

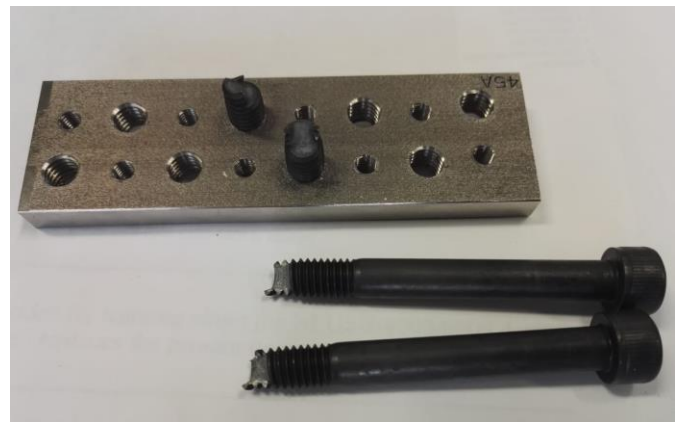


Figure 18: Thread-stripping results with 12.9 bolts

3.7 Thread profiles

All the M5 and M8 internal threads, regardless of printing orientation and heat treatment, were successfully tapped in maraging steel. The tapping process was followed by the removal of burrs from the threads, after which the threads passed the go/no go testing.

In the case of pre-hole diameters that were smaller than the nominal diameter, i.e., 4.2 mm and 6.8 mm, the thread profile was free of porosity and had fine sharp edges.

In order to depict the worst-case scenario, this study focuses on the M5 thread profiles of the largest pre-hole diameter, i.e., 4.3 mm. The results of the M8 thread profiles were in line with those of the M5. Further, the investigation focuses on the

plates printed at 0° and 90° inclinations to represent the highest or minimum impact of the inclination range. The effect of dross, which undermines the thread strength/profile, would be the highest for the largest pre-holes as a result of a lack of adequate drilling. In this case, the down-skin thread had a loss of material and a lack of sharp edges. This is due to the formation of dross at the down-skin surfaces. Though the dross was removed through drilling, its porosity remained in the bulk of the material. Figure 19 shows the M5 and M8 internal threads cut in one of the ST plates.



Figure 19: M5 and M8 threads in ST maraging steel plate

In the case of the AB plate (Figure 20), the thread profiles, including the crest, flank, and root, are sharp because they do not include either the down-skin or up-skin surfaces at a 0° inclination. The exposure parameters of the down-skin and up-skin differ from each other, as well as the bulk of the material, because of the gravitational forces acting on the melt pool on the down-skin and on the un-melted powder above the up-skin surfaces. However, these measures only mitigate the occurrence of defects which are likely to occur, even if they are insignificant.

At a 90° inclination, the up-skin and down-skin thread profiles, shown in Figures 21 and 22, lack sharpness compared to a 0° inclination. The intensity in the lack of sharpness is greater for down-skin threads than the up-skin thread. The down-skin thread profile is predominantly affected by the formation of dross. The up-skin thread can be affected by several factors, i.e., inadequate removal of the material from the crest through drilling and tapping as a result of a larger pre-hole than the nominal diameter coupled with non-uniform shrinkage and the deformation of the crest caused by the weight of the powder on top acting as an insulator. Additionally, the flank of the up-skin thread can be affected by brittle fractures in some cases, which remove excessive material through cracking.

Figure 23 shows a good-quality thread with a sharp profile in the case of an ST plate at a 0° inclination. At a 90° inclination, the up-skin (Figure 24) and down-skin (Figure 25) threads yield inferior-quality threads in the worse cases.

The flank of the up-skin thread is probably affected by excessive brittle fractures, and the crest is affected by inadequate removal of the material through drilling and tapping. Further, the deformation caused by the weight of the un-melted powder on top can also have an impact on the crest through further deformation during the solution treatment. The down-skin thread profile is mainly affected by the lack of

material resulting from the formation of dross, which worsened after the solution treatment.

This can be avoided by introducing smaller pre-holes compared to the nominal diameter, which would allow the removal of unwanted effects of dross at the down-skin and deformation effects at the up-skin through the drilling process. Ullah et al. [25] have recommended a machining allowance of 0.3 mm, mainly due to the presence of outer contours in the scan strategy, to ensure the removal of such defects for additively manufactured aluminum. As a result of this study, the 0.3-mm machining allowance can also be applied to additively manufactured maraging steel.

Figures 26-29 show superior-quality thread profiles for the aged plates regardless of their initial condition, i.e., AB and ST, and location of the thread, i.e., up-skin and down-skin. The results confirm that sharp threads can be manufactured in high-strength maraging steel in a hardened state. No significant tool wear was observed in the machining of the aged plates.

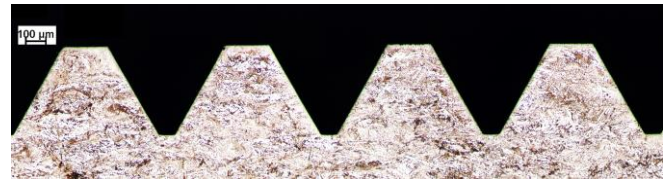


Figure 20: AB plate, M5, pre-hole diameter 4.3 mm, objective 10 X, 0° printing inclination



Figure 21: AB plate, M5, pre-hole diameter 4.3 mm, up-skin thread, objective 10 X, 90° printing inclination



Figure 22: AB plate, M5, pre-hole diameter 4.3 mm, down-skin thread, objective 10 X, 90° printing inclination

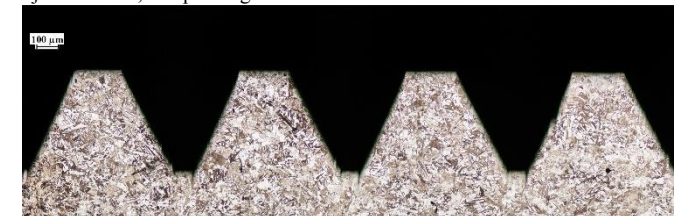


Figure 23: ST plate, M5, pre-hole diameter 4.3 mm, objective 10 X, 0° printing inclination



Figure 24: ST plate, M5, pre-hole diameter 4.3 mm, up-skin thread, objective 10 X, 90° printing inclination



Figure 25: ST plate, M5, pre-hole diameter 4.3 mm, down-skin thread, objective 10 X, 90° printing inclination

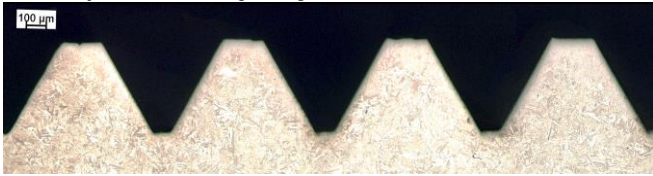


Figure 26: ST+Aged, M5, pre-hole diameter 4.3 mm, up-skin thread, objective 10 X, 90° printing inclination

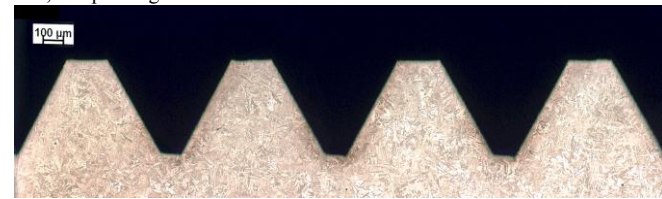


Figure 27: ST+Aged, M5, pre-hole diameter 4.3 mm, down-skin thread, objective 10 X, 90° printing inclination



Figure 28: AB+Aged, M5, pre-hole diameter 4.3 mm, up-skin thread, objective 10 X, 90° printing inclination



Figure 29: AB+Aged, M5, pre-hole diameter 4.3 mm, down-skin thread, objective 10 X, 90° printing inclination

Conclusions

This study evaluated anisotropy in the part properties of additively manufactured maraging steel. The design of the test plate enabled a unified method of analyzing flatness, surface roughness, surface hardness, pre-hole shrinkage, drilling thrust force, and thread profiles. The test plates were additively manufactured using the EOS Performance 2.0 parameter set. The effect of AB plates and ST plates was investigated for the printing orientations at five inclinations. The effect of aged plates was also evaluated for the worst-case scenario.

On the basis of the results, we draw the following conclusions.

- i. The flatness error increases in the following inclination order: 90°, 0°, 60°, 45°, and 30°, owing to the heat transfer capability in terms of the maximum energy input per layer and the cross-sectional area of support structures that also anchors the part to the substrate. The

solution treatment can significantly reduce the flatness error.

- ii. The surface roughness decreases from a 30° to a 60° inclination as a result of the staircase effect coupled with the powder conglomeration. It was slightly smaller at a 90° inclination because of the absence of a stair-case geometry leading to a lessened degree of powder conglomeration. It was at its minimum at a 0° inclination owing to the immunity from the staircase effect and due to the relatively lowest degree of powder conglomeration. The solution treatment can increase the surface roughness compared to as-built parts because of the oxidation effect occurring at elevated temperatures.
- iii. The EOS Performance 2.0 parameter set enabled quite uniform surface hardness as a function of the printing inclination indicating isotropic behavior for the as-built (within a range of 1.13 HRC with a STD of 0.44 HRC) and solution-treated (within a range of 0.92 HRC with a STD of 0.37 HRC) parts. The solution treatment can reduce the hardness by approximately 20% in contrast to the as-built parts owing to the coarseness in the morphology of the microstructure. The aging process can increase the hardness of the as-built parts by around 48% and solution-treated parts by around 86% to yield uniform hardness for both initial phases.
- iv. All the additively manufactured pre-holes underwent an average shrinkage of 150 µm for the 4.2-mm pre-hole, whereas an increase of 13% was observed in the 6.8-mm pre-hole. No significant difference in the shrinkage was observed when the printing inclination was changed and when solution treatment was applied. All the down-skin surfaces of the pre-holes contained dross, which increased from a 0° to a 90° inclination.
- v. No significant fluctuation in the drilling thrust force was observed when the printing inclination was changed. The drilling thrust force largely depends on the pre-hole diameter. A machining allowance of 0.4 mm to 3.8 mm can reduce the thrust force by around 92% and 59% for the 4.2-mm drill. Similarly, a machining allowance of 0.4 mm to 2.4 mm can reduce it by around 90% and 54% for the 6.8-mm drill. The solution treatment can reduce the drilling thrust force by approximately 5% for a 4.2-mm drill and 8% for a 6.8-mm drill. The aging treatment increases the drilling thrust force by 51% compared to an as-built part and 58% compared to a solution-treated part. A large drilling thrust force can be critical for the structural integrity of weak features of a part, and it can potentially cause tool wear that can contribute to accumulating costs.
- vi. All the M5 and M8 internal threads, regardless of printing orientation and heat treatment, were successfully tapped and passed the go/no-go testing. Because of the high strength of the maraging steel, the custom-made setup was unable to strip the threads and resulted in fractured taps. In the case of pre-hole diameters that were smaller than the nominal diameter, the thread profile had good quality and was free of porosity. A pre-hole diameter that was larger than the nominal diameter

enabled the evaluation of possible defects that were observed only in several sections of the down-skin and up-skin surfaces of the threads. The down-skin profile of the as-built thread is predominantly affected by the lack of material resulting from the formation of dross, which worsened for the threads tapped in the solution-treated parts. Comparatively, the up-skin is affected to a lower degree as a result of several factors, i.e., inadequate removal of the material through drilling and tapping, non-uniform shrinkage, deformation caused by the weight of the powder on top, and brittle fractures during tapping. In the case of the aged parts, the thread profile had good quality and was free of porosity and deformations for even the down- and up-skin surfaces. Designers should consider implementing a machining allowance of 0.3 mm to ensure the removal of the unwanted effects of dross at the down-skin and deformation effects at the up-skin through the drilling process.

Acknowledgements

The authors would like to acknowledge Roy Björkstrand (Aalto University) and Antti Seppala (EOS Finland) for valuable discussions. Special thanks are extended to the staff of EOS Finland for providing the additively manufactured parts. This research was funded by the FIN3D project at the Department of Mechanical Engineering, Aalto University, Finland.

Author contributions: The work was accomplished according to the ICMJE authorship guidelines, which comply with ethical standards.

Conflict of interest: None declared.

References

- [1]. Mouritz AP, editor. 11 - Steels for aircraft structures. *Introd. Aerosp. Mater.*, Woodhead Publishing; 2012, p. 232–50.
- [2]. Garcia-Mateo C, Caballero FG. 1.09 - Advanced High Strength Bainitic Steels. In: Hashmi S, Batalha GF, Van Tyne CJ, Yilbas B, editors. *Compr. Mater. Process.*, Oxford: Elsevier; 2014, p. 165–90.
- [3]. Akmal JS, Salmi M, Mäkitie A, Björkstrand R, Partanen J. Implementation of Industrial Additive Manufacturing: Intelligent Implants and Drug Delivery Systems. *J Funct Biomater* 2018;9.
- [4]. ISO/ASTM 52900(en), Additive manufacturing — General principles — Terminology n.d. <https://www.iso.org/obp/ui/#iso:std:iso-astm:52900:dis:ed-2:v1:en> (accessed November 23, 2019).
- [5]. kokkonen P, Salonen L, Virta J, Hemming B, Pasi L, Savolainen M, et al. Design guide for additive manufacturing of metal components by SLM process. Espoo: VTT; n.d.
- [6]. Mohammadi M, Asgari H. Achieving low surface roughness AlSi10Mg_200C parts using direct metal laser sintering. *Addit Manuf* 2018;20:23–32.
- [7]. Ning Y, Wong YS, Fuh JYH, Loh HT. An approach to minimize build errors in direct metal laser sintering. *IEEE Trans Autom Sci Eng* 2006;3:73–80.
- [8]. Dai K, Shaw L. Finite element analysis of the effect of volume shrinkage during laser densification. *Acta Mater* 2005;53:4743–54.
- [9]. Huang Y, Yang LJ, Du XZ, Yang YP. Finite element analysis of thermal behavior of metal powder during selective laser melting. *Int J Therm Sci* 2016;104:146–57.
- [10]. Li L, Haghighi A, Yang Y. A novel 6-axis hybrid additive-subtractive manufacturing process: Design and case studies. *J Manuf Process* 2018;33:150–60.
- [11]. Qian C, Zhang Y, Liu Y, Wang Z. A cloud service platform integrating additive and subtractive manufacturing with high resource efficiency. *J Clean Prod* 2019;241:118379.
- [12]. Chen N, Frank M. Process planning for hybrid additive and subtractive manufacturing to integrate machining and directed energy deposition. *Procedia Manuf* 2019;34:205–13.
- [13]. Suzuki A, Nishida R, Takata N, Kobashi M, Kato M. Design of laser parameters for selectively laser melted maraging steel based on deposited energy density. *Addit Manuf* 2019;28:160–8.
- [14]. Azizi H, Ghiaasiaan R, Prager R, Ghoncheh MH, Samk KA, Lausic A, et al. Metallurgical and mechanical assessment of hybrid additively-manufactured maraging tool steels via selective laser melting. *Addit Manuf* 2019;27:389–97.
- [15]. Du W, Bai Q, Zhang B. Machining characteristics of 18Ni-300 steel in additive/subtractive hybrid manufacturing. *Int J Adv Manuf Technol* 2018;95:2509–19.
- [16]. Fortunato A, Lulaj A, Melkote S, Liverani E, Ascari A, Umbrello D. Milling of maraging steel components produced by selective laser melting. *Int J Adv Manuf Technol* 2018;94:1895–902.
- [17]. Bai Y, Yang Y, Wang D, Zhang M. Influence mechanism of parameters process and mechanical properties evolution mechanism of maraging steel 300 by selective laser melting. *Mater Sci Eng A* 2017;703:116–23.
- [18]. Mutua J, Nakata S, Onda T, Chen Z-C. Optimization of selective laser melting parameters and influence of post heat treatment on microstructure and mechanical properties of maraging steel. *Mater Des* 2018;139:486–97.
- [19]. Casalino G, Campanelli SL, Contuzzi N, Ludovico AD. Experimental investigation and statistical optimisation of the selective laser melting process of a maraging steel. *Opt Laser Technol* 2015;65:151–8.
- [20]. Song J, Tang Q, Feng Q, Ma S, Setchi R, Liu Y, et al. Effect of heat treatment on microstructure and mechanical behaviours of 18Ni-300 maraging steel manufactured by selective laser melting. *Opt Laser Technol* 2019;120:105725.
- [21]. EOS Metal Materials for Additive Manufacturing n.d. <https://www.eos.info/material-m> (accessed March 26, 2020).
- [22]. Mooney B, Kourousis KI, Raghavendra R. Plastic anisotropy of additively manufactured maraging steel: Influence of the build orientation and heat treatments. *Addit Manuf* 2019;25:19–31.
- [23]. Bai Y, Wang D, Yang Y, Wang H. Effect of heat treatment on the microstructure and mechanical properties of maraging steel by selective laser melting. *Mater Sci Eng A* 2019;760:105–17.
- [24]. Yao Y, Zhu H, Huang C, Wang J, Zhang P, Yao P. Investigation on chip formation and surface integrity in micro end milling of maraging steel. *Int J Adv Manuf Technol* 2019;102:1973–84.
- [25]. Ullah R, Akmal JS, Laakso SVA, Niemi E. Anisotropy of additively manufactured AlSi10Mg: Threads and surface integrity. *Int J Adv Manuf Technol* 2019: Accepted.
- [26]. Material data sheet. EOS Maraging Steel MS1 https://cdn0.scrvt.com/eos/c88047245bff2c4b/2f494ef432d0/MS1-MS1-M280_M290_400W_Material_data_sheet_05-14_en.pdf
- [27]. Walter Tools » Engineering Kompetenz <https://www.walter-tools.com/en-gb/pages/default.aspx> (accessed June 9, 2019).
- [28]. Katz Z, Poustie A. On the Hole Quality and Drill Wandering Relationship. *Int J Adv Manuf Technol* 2001;17:233–7.